

Article

Influence of Electrical Stimulation on the Friction Performance of LiPF₆-Based Ionic Liquids

Xiangyu Ge ¹, Xiaodong Wu ¹, Qiuyu Shi ^{2,*}, Yanfei Liu ^{1,*} and He Liang ¹

¹ School of Mechanical Engineering, Beijing Institute of Technology, Beijing 100081, China; gexy@bit.edu.cn (X.G.); wuxd_me@163.com (X.W.); lianghe@bit.edu.cn (H.L.)

² State Grid Smart Grid Research Institute Co., Ltd., Beijing 102209, China

* Correspondence: shiqiuyu@geiri.sgcc.com.cn (Q.S.); liuyanfei@bit.edu.cn (Y.L.)

Abstract: This work studied the influence of the voltage parameters on the friction and superlubricity performances of LiPF₆-based ionic liquids (ILs). The results show that the voltage direction and magnitude greatly affected the friction performances of ILs and that macroscale superlubricity can be achieved with a stimulation of -0.1 V. The surface analysis and experiment results indicate that the voltage magnitude influences the coefficient of friction (COF) by determining the types of substances in the tribochemical film formed on the ball, while the voltage direction influences the COF by affecting the adsorption behavior of Li(PEG)⁺ ions on the ball. At -0.1 V, the cation group Li(PEG)⁺ adsorption film and FeOOH-containing tribochemical film contribute to friction reduction. The formation of Fe_xO_y within the tribochemical film results in an increase in friction at -0.8 V. The limited adsorption of Li(PEG)⁺ ions and the formation of Fe_xO_y contribute to the elevated COF at $+0.1$ V. This work proves that the friction performances of LiPF₆-based ILs could be affected by voltage parameters. A lubrication model was proposed hoping to provide a basic understanding of the lubrication mechanisms of ILs in the electric environment.

Keywords: superlubricity; ionic liquids; electrical stimulations; voltage



Citation: Ge, X.; Wu, X.; Shi, Q.; Liu, Y.; Liang, H. Influence of Electrical Stimulation on the Friction Performance of LiPF₆-Based Ionic Liquids. *Lubricants* **2024**, *12*, 167.

<https://doi.org/10.3390/lubricants12050167>

Received: 27 March 2024

Revised: 6 May 2024

Accepted: 8 May 2024

Published: 9 May 2024



Copyright: © 2024 by the authors. Licensee MDPI, Basel, Switzerland. This article is an open access article distributed under the terms and conditions of the Creative Commons Attribution (CC BY) license (<https://creativecommons.org/licenses/by/4.0/>).

1. Introduction

Amidst a worsening global energy crisis, the demand for electromechanical systems is rapidly increasing [1]. However, the shaft voltages and currents generated during the operation can lead to premature failure of components such as bearings, gears, seals, and gaskets, thereby affecting the overall lifespan [2,3]. Therefore, investigating the friction performance influenced by electrical stimulation at steel interfaces is of significant engineering importance [4]. When the sliding coefficient of friction (COF) is below 0.01, an optimal lubrication state known as superlubricity [5,6] is achieved, resulting in substantial reductions in energy loss and wear compared to conventional lubrication.

Currently, the superlubricity materials include 2D materials [7–11], coatings [12,13], salts and ionic liquids (ILs) [14–16], oil-based solutions [17–19], polyol solutions [20,21], and biological mucus [22]. Researchers have been working to extend superlubricity to electrical environments and successfully demonstrated microscale superlubricity with various materials with electrical stimulation [23,24]. Rob Atkin et al. [25] realized superlubricity at the silicon–graphite interface with the lubrication of ILs in an electrical environment. The observed superlubricity is attributed to a significant reduction in energy dissipation when an atomic force microscope (AFM) tip scans an anion-rich interface under electrical conditions. They demonstrated that the occurrence of superlubricity could be altered by changing the direction of electrical stimulations. Zhang et al. [26] discovered that the metal cations in polyethylene phosphonic acid play a crucial role in microscale superlubricity. By modifying the cation radius, the adhesion force between the tribo-pairs was altered, thereby influencing the friction force and achieving superlubricity. However, superlubricity

in an electrical environment is predominantly achieved at the microscale, and macroscale superlubricity achievement in an electrical environment remains a challenge. Therefore, it is essential to investigate the influence of electrical stimulation on the friction performance of lubricants and elucidate the underlying mechanisms.

Liu et al. pioneered research on ionic liquids (ILs) as lubricants, highlighting their remarkable tribological performance in 2001 [27]. They attributed this performance to the distinctive structure of ILs, which enables their adsorption onto frictional surfaces. Subsequent reactions were observed, leading to the generation of fluorides, B_2O_3 , and BN substances. Since then, ILs have been extensively studied as lubricants and additives under electrical stimulations [28]. Ramezani et al. [29] provided a review of methods for achieving superlubricity with ILs at both the nanoscale and macroscale, highlighting the influence of external conditions. Kustov et al. [30] conducted a comparative overview comparing polymeric ionic liquids (PILs) with other polymers and materials, emphasizing the advantages of PILs in multiple applications such as lubrication. Xia et al. [31] investigated the friction behavior of ILs under voltage stimulation. The results show that IL not only greatly reduces the COF, ECR, and wear widths but also makes them more stable as compared with multiply-alkylated cyclopentanes under voltage stimulations. Moreover, the higher the voltage, the lower the COF value. They found that the excellent tribological behaviors of ILs are attributed to their high conductivity and the complex protective film generated on worn surfaces. Amann et al. [32] demonstrate that the application of electric stimulation induces a permanent alteration in the frictional response when lubricated with ILs. This alteration is presumably attributed to variations in the externally induced electrical polarization at the surface, which, in turn, affects molecular adsorption, the exchange of adsorbed ions, and their molecular orientation. Tian et al. [33] studied the effect of electric potential on lubrication performance, revealing that the potential alters lubrication efficacy by modulating the types and concentrations of adsorbed ions.

In summary, the friction behavior of ILs can be regulated by electric stimulations and has been proven capable of achieving macroscopic superlubricity in non-electric environments. Therefore, ILs hold the potential for macroscopic superlubrication by electric stimulation, motivating our research efforts in this area.

2. Materials and Methods

2.1. Materials and Preparation

According to our previous research results [34], polyethylene glycol with a number average molecular weight of 200 (PEG200) was chosen as the base oil, and the lithium salt $LiPF_6$ was chosen as the additive. The PEG200 was supplied by Aladdin Company, and the $LiPF_6$ was supplied by Dow Chemical Co., Ltd, Midland, MI, USA. All the involved chemical materials had a 99% purity and no additional treatment was employed. The IL was synthesized by combining $LiPF_6$ salt with PEG at a specific ratio of 0.8 wt%. During the blending process, the lone electron pairs on the oxygen atoms of PEG molecules interacted with Li^+ cations, leading to the formation of $Li(PEG)^+$ cations. These cations were then combined with PF_6^- anions to form the $Li(PEG)PF_6$ IL [35,36] (Figure 1a). The conductivity of the $Li(PEG)PF_6$ solution was measured by a DDS-307A conductivity meter. The viscosity value of the synthetic IL was measured at room temperature using a rheometer (MCR101, Anton Paar, Graz, Austria).

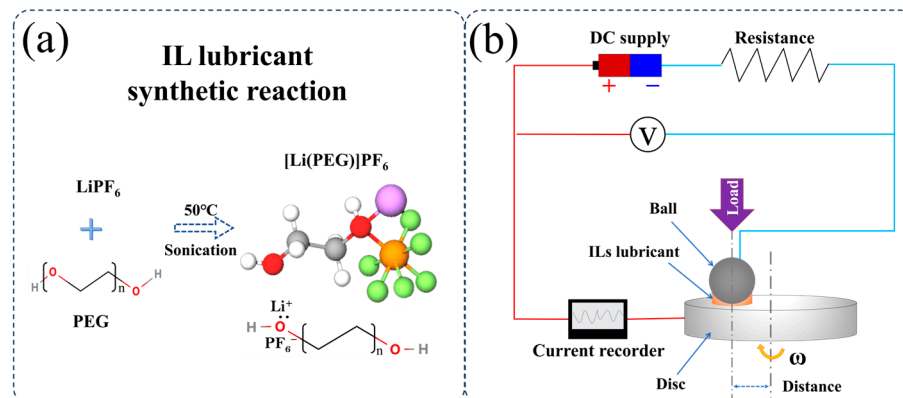


Figure 1. (a) IL lubricant synthetic reaction, (b) sketch of test equipment.

2.2. Frictional Tests

Frictional experiments were conducted on a universal micro-tester (UMT-3, Bruker, Karlsruhe, Germany). Additional equipment was designed based on the two-electrode cell principle to administer electrical stimulation to the tribological pair (Figure 1b). When the ball acted as the positive terminal of the direct current supply while the disc acted as the negative terminal, the voltage was regarded as positive. Conversely, when the ball functioned as the negative terminal and the disc as the positive terminal, the voltage was treated as negative. The tribo-pair consisted of a GCr15 ball (Ø 10 mm, surface roughness (R_q) about 10 nm) and a GCr15 disc (R_q about 15 nm). All tests were conducted at room temperature with a relative humidity exceeding 30%. The relative sliding velocity (0.23 m/s) and the load (2 N) were kept constant in each friction test. Before each test, the balls and discs underwent ultrasonic cleansing with ethanol and pure water (each for 15 min) and were then dried using a nitrogen flow. During each test, 20 μL of liquid was dispensed onto the contact area. The COF was automatically processed and displayed by a computer. Each test was conducted thrice, and the average COF value with an error bar was reported; the COF measurement accuracy was within ± 0.001 . The platform's levelness and the loading device's verticality were altered to ensure consistent COF values during clockwise and counterclockwise rotations.

2.3. Surface Analysis

After the friction test, the wear scar diameter (WSD) and R_q of the ball's wear area were measured by a microscope and a 3D white light interferometer (Nexview, Zygo Lambda, Middlefield, CT, USA), respectively. The surface topography of the worn surfaces was observed by a scanning electron microscope (SEM, S4800, Hitachi, Tokyo, Japan). An X-ray photoelectron spectroscope (XPS, PHI QUANTERA-II SXM, Ulvac-Phi, Chigasaki, Japan) and a Raman spectrometer (LabRAM HR Evolution, HORIBA Scientific, Paris, France) were used to characterize the chemical state of the worn surfaces.

3. Results

The friction performances of $\text{Li}(\text{PEG})\text{PF}_6$ (with a conductivity of $94 \mu\text{S}/\text{cm}$) as the lubricant under various electrical stimulations were studied (Figure 2a). In the case of 0 V, the COF stabilizes at 0.018 after a running-in stage of 200 s. In the case of +0.1 V, a stable lubricating state is achieved post-160 s, and the stable COF is about 0.021. In the case of -0.8 V, the COF stabilizes at 0.020 after a running-in stage of 200 s. In the case of -0.1 V, the COF stabilizes at about 0.009 after a running-in stage of 150 s. These friction results show that the COF obtained under -0.1 V stimulation was much smaller than that under other electrical stimulations and that a superlubricity state was achieved.

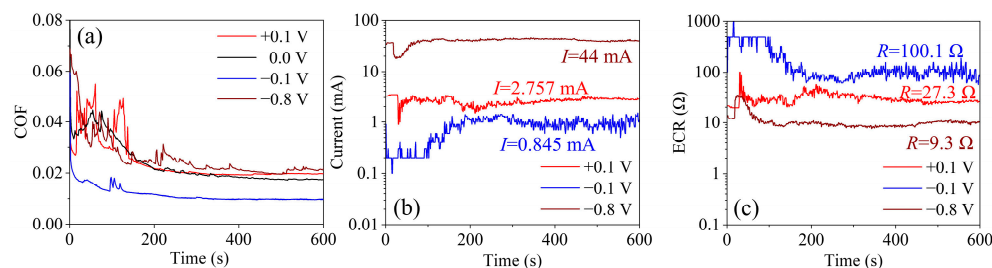


Figure 2. (a) The COFs of ILs, (b) current, and (c) ECR under various electrical stimulations at 0.23 m/s and 2 N.

The current signals during friction tests were recorded by a current recorder connected to the circuit (Figure 2b). Results show that the average currents during the stable stage were 44 mA (−0.8 V), 0.845 mA (−0.1 V), and 2.757 mA (+0.1 V), corresponding to an electric contact resistance (ECR) of 9.3, 100.1, and 27.3 Ω, respectively (Figure 2c). In all electrical stimulations, there was an instability stage in the ECR evolution, which was in conjunction with the running-in stage of the COF curve. Under −0.1 V stimulation, the ECR remained stable at about 100.1 Ω after the instability stage of 200 s. When exposed to +0.1 V stimulation, the stable ECR value was about 27.3 Ω after 200 s. When the electrical stimulation was +0.8 V, the ECR stabilized at about 9.3 Ω after the instability stage of 150 s. It is worth noting that there is a positive correlation between the COF and the change in the ECR value during the friction process. The ECR obtained at −0.1 V is larger compared to +0.1 V and −0.8 V. This difference could be attributed to the formation of specific compounds or film thickness during the sliding process, which, in turn, contributes to the smaller COF value. Therefore, the physical and chemical properties of the worn surfaces were investigated.

4. Discussion

To elucidate the effect of electrical parameters on friction performance, the WSDs and worn surface topography were investigated. The WSDs at −0.8, −0.1, 0, and +0.1 V are 237, 124, 224, and 194 μm, respectively. The corresponding contact stresses are 36, 130, 40, and 53 MPa. This indicates that both the COF and wear are minimized at −0.1 V. With SEM observation, only furrows appeared on the worn surface resulting from stimulation at −0.1 V (Figure 3f). These furrows comprised small pits with a diameter of less than 10 μm (Figure 3j). Conversely, when stimulated at −0.8, 0, and +0.1 V, large pits were also evident alongside furrows. The diameter of these large pits ranged from 10 to 20 μm, with a few exceeding 20 μm. The analysis concludes that disc-worn surfaces exhibit both large and small pits when stimulated with 0, −0.8, and +0.1 V. However, only small pits are observed on the disc-worn surface when stimulated with −0.1 V. This implies that preserving small pits while eliminating large ones would contribute to reducing friction. To evaluate the lubrication condition, the surface roughness of the worn surfaces under various voltage stimulations was measured (Figure 4). Notably, the ball surface roughness remains almost identical across cases of 0, −0.1, and −0.8 V, whereas it diminishes at +0.1 V. Conversely, the disc surface roughness exhibits minimal variation across all cases. Within the involved voltage range, negative voltages show negligible impact on the surface roughness, whereas positive voltage decreases the ball surface roughness.

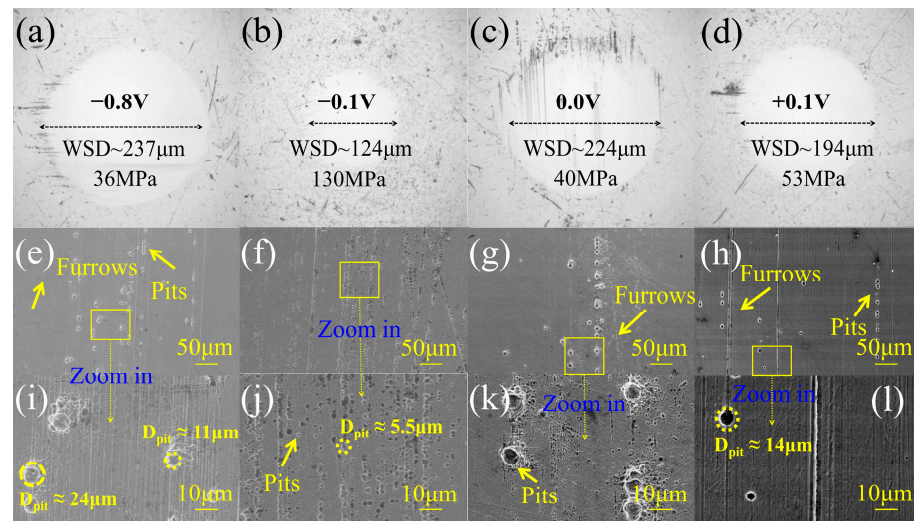


Figure 3. SEM images of worn surfaces under different electrical stimulations; (a–d) ball-worn surfaces, (e–h) disc-worn surfaces under low magnification (1000×), and (i–l) disc-worn surfaces under high magnification (5000×).

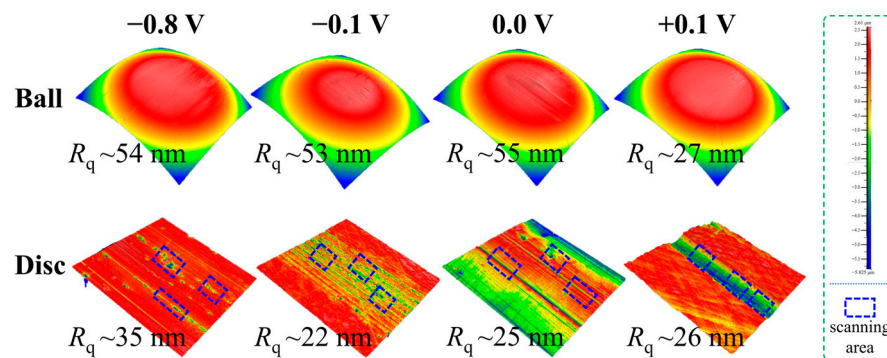


Figure 4. Three-dimensional white-light images of worn surfaces under different electrical stimulations.

The H-D formula [37] (Equation (1)) was employed to estimate the fluid film thickness in a stable lubrication state:

$$h_c = 2.69 \frac{Q^{0.53} R S^{0.67}}{M^{0.067}} \left(1 - 0.61e^{-0.73c}\right), \quad (1)$$

where $Q = \kappa E'$, $S = \eta u / E' R$, $M = w / E' R^2$, and κ is the viscosity–pressure coefficient (7 GPa^{-1}). In the H-D formula (Equation (1)), η represents the dynamic viscosity ($47.79 \text{ mPa}\cdot\text{s}$), u denotes the average relative sliding velocity of the tribo-pair (117 mm/s), w signifies the normal load (2 N), c stands for a constant coefficient (typically 1), and E' indicates the equivalent elastic modulus of the surface material, calculated by Equation (2),

$$E' = 2 / \left[\left(1 - \nu_1^2\right) / E_1 + \left(1 - \nu_2^2\right) / E_2 \right], \quad (2)$$

where E_1 and E_2 represent the elastic modulus of GCr15 (208 GPa) and ν_1 and ν_2 denote the Poisson's ratio of GCr15 (0.3). To derive the effective contact radius (R), the WSD on the ball was assumed to follow the Hertz elastic contact deformation under the normal load. Subsequently, the WSD was characterized using Equation (3),

$$\frac{d}{2} = \left(\frac{3Rw}{4E''} \right)^{\frac{1}{3}}, \quad (3)$$

Thus, the effective contact radius was estimated by Equation (4),

$$R = \frac{E'' d^3}{6\omega}, \quad (4)$$

where E'' represents the effective comprehensive elastic modulus of the tribo-pair material,

$$E'' = 1 / \left[\left(1 - \nu_1^2\right) / E_1 + \left(1 - \nu_2^2\right) / E_2 \right], \quad (5)$$

The lubrication state was categorized based on the film thickness ratio, as described in Equation (6),

$$\lambda = \frac{h_c}{\sqrt{\sigma_1^2 + \sigma_2^2}} \quad (6)$$

The fluid film thickness and the film thickness ratio are listed in Table 1. The results indicate that, under all the electrical stimulation conditions, the film thickness ratios are larger than 1 and smaller than 3. This suggests that the lubrication state is mixed lubrication (ML) during stable lubrication; namely, the boundary film and the fluid film coexist at the interfaces.

Table 1. Film thickness (h_c) and film thickness ratio (λ) for stable lubrication conditions under different electrical stimulations.

Voltages (V)	−0.8	−0.1	0.0	+0.1
Fluid film thickness ($h_c/\mu\text{m}$)	150	61	139	114
Film thickness ratio (λ)	2.3	1.1	2.3	2.9
Lubrication state	ML	ML	ML	ML

XPS was employed to characterize the chemical state of the worn surface, aiming to delve deeper into the composition of the boundary film. The chemical state of the disc-worn surfaces after being tested under various voltage stimulations was studied (Figure 5). The C1s scans show that the products on the disc-worn surface contain C-C/C-H (284.8 eV) [38], C-F (287.0, 288.2, and 288.5 eV) [39–42], and C-O (284.53, 285.5, and 286.0 eV) [43,44] bonds, and that there is no significant difference in C1s scans for all conditions. In addition, the O1s, Li1s, and P2p scans on the disc-worn surface under each voltage stimulation show no difference in their corresponding tribochemical products, including FeOOH (531.7 eV), Fe_xO_y (530.0 eV) [45], Li^+ (55.7 eV) [46], and P-O (133.3 eV) [46]. The similar XPS results indicate that the relevant tribochemical products on the disc-worn surface have the same composition. However, the F1s scans at ± 0.1 V and -0.8 V indicate the presence of LiF on the worn surfaces of discs, suggesting that new LiF substances were generated under electrical stimulations compared to that under 0 V. The LiF peak for -0.1 V was the strongest, indicating that more LiF (0.22%) was generated on the disc-worn surface after testing at -0.1 V and might be beneficial for friction reduction. The above results indicate that the direction and magnitude of voltage stimulation have little effect on the type of electrochemical products on the disc-worn surfaces.

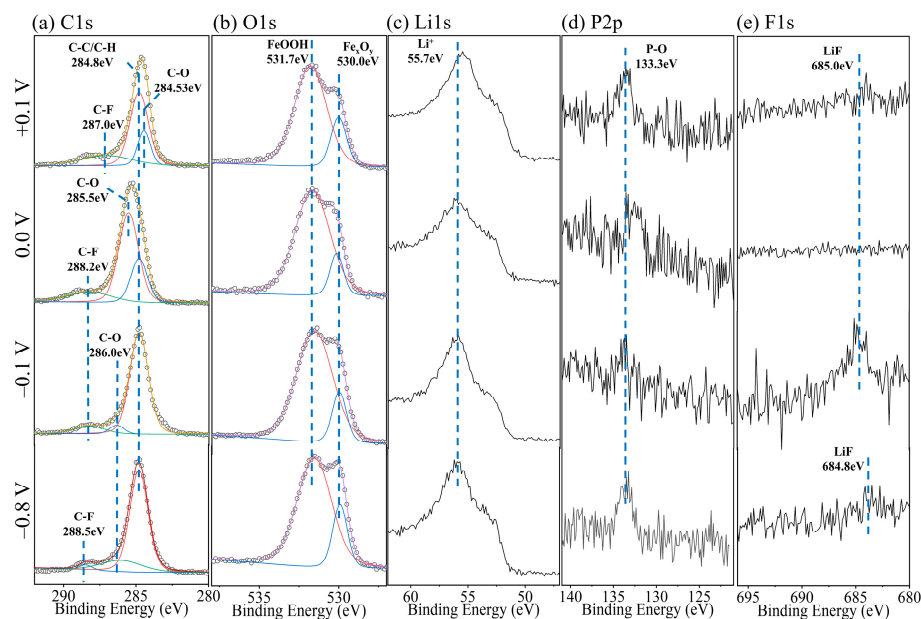


Figure 5. XPS scan results on the discs under different electrical stimulations, (a) C1s, (b) O1s, (c) Li1s, (d) P2p, and (e) F1s.

The spectra of the basic elements of C and O on the ball-worn surfaces are shown in Figure 6a. After the friction test conducted under 0 V, the C1s scan of the ball-worn surface indicates the presence of C-C/C-H (284.8 eV), C-O (284.3 eV), and C-F (288.0 eV). The O1s scan indicates the presence of FeOOH (531.7 eV) and Fe_xO_y (530.0 eV). In the case of +0.1 V, the C1s scan indicates that only C-C/C-H (284.8 eV) and C-F (288.0 eV) are present on the ball-worn surface. The absence of C-O compared to the 0 V condition indicates the difficulty of Li(PEG)⁺ ions adsorption on the ball under positive voltage stimulation. The O1s scan results are similar to those at 0 V, with only FeOOH and Fe_xO_y present. In the case of −0.1 V, the C1s scan results indicate the presence of C-C/C-H (284.8 eV), C-O (285.0 eV), and C-F (288.0 eV) on the ball-worn surface. The O1s scan shows that only FeOOH is present on the ball, with no detectable peak of Fe_xO_y. In the case of −0.8 V, the products on the ball-worn surface are complex. The C1s scan indicates the presence of C-C/C-H (284.8 eV), C-O (284.3 eV), C-F (288.0 eV), and Cr₃C₂ (283.2 eV). The O1s scan manifests the presence of C=O (535.1 eV), C-O (532.5 eV), FeOOH (531.2 eV), and Fe_xO_y (530.7 eV) on the ball-worn surface. The spectra of the elements from LiPF₆ are shown in Figure 6b. The Li1s scan shows the presence of Li⁺ (55.7 eV) on the ball-worn surfaces after the friction test that was conducted in all conditions. In the P2p scan, no peaks are observed on the ball-worn surfaces, on which the friction test was conducted at 0 V and ±0.1 V, while only P-O bonds (133.3 eV) are detected after being tested at −0.8 V. No peaks are observed in the F1s scan for all conditions. These results indicate that the direction and magnitude of the voltage determine the types of products generated on the ball-worn surfaces during the friction process. Combined with the friction test results, we speculate that the effect of voltage stimulation on the tribochemical film and the adsorption film on the ball is the main factor that influences the COF. Compared to the lowest COF obtained under −0.1 V stimulation, the increase in COF under −0.8 V conditions may be attributed to the formation of a tribochemical film containing multiple substances on the ball-worn surface. Under +0.1 V conditions, the increase in COF may be due to the excessive formation of iron oxide and the lack of Li(PEG)⁺ ions adsorption (no C-O peak).

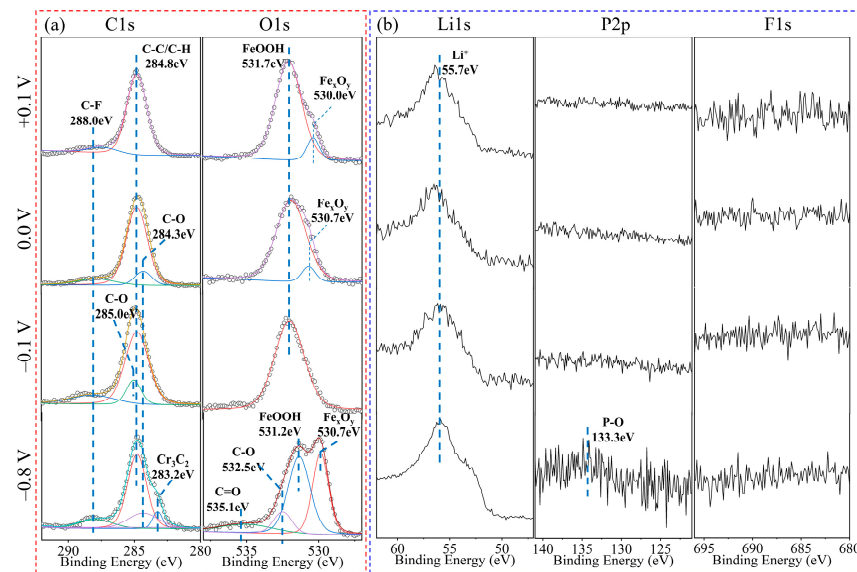


Figure 6. XPS scan results on the ball-worn surfaces under different electrical stimulations. (a) Basic element: C1s and O1s; (b) Li salt element: Li1s, P2p, and F1s.

To validate the hypothesis that the voltage stimulation's effect on the ball is the primary factor influencing the COF, a supplementary friction test was designed and conducted. As shown in Figure 7a, an initial friction test was conducted at -0.1 V until a stable lubrication condition was achieved, and the worn ball was retained. Subsequently, a friction test at -0.8 V was carried out on a new tribo-pair until a stable lubrication condition was achieved (Figure 7b). The test was then paused, maintaining the disc and residual lubricant as unchanged. The ball used in the -0.8 V test was replaced with the one retained from the -0.1 V test. The friction test at -0.8 V was then resumed using the same worn tracks on the ball and disc (Figure 7c). The results (Figure 7d) indicate that the COF stabilized at 0.021 under -0.8 V before the ball replacement. Shortly after the replacement, the COF sharply decreased to around 0.017 and remained stable for about 150 s before rising to 0.042. This suggests that the boundary film on the ball (from the -0.1 V test) exhibited better antifriction performance after the ball replacement, leading to a reduced COF for 150 s, consistent with the initial hypothesis. The sudden change in the COF after 150 s may be attributed to the small WSD of the ball (from the -0.1 V test) and the mismatched disc-worn surface, resulting in increased contact pressure and a new running-in stage, which in turn led to the breakdown of the boundary film on the ball.

Based on the above results and analysis, a lubrication model under voltage stimulation was established (Figure 8). The voltage magnitude influences the COF by determining the types of substances in the tribochemical film formed on the ball, while the voltage direction influences the COF by affecting the adsorption behavior of Li(PEG)^+ ions on the ball. At -0.1 V (the optimal voltage), the steel ball was the negative terminal. Cation group Li(PEG)^+ ions adsorb onto the ball via electrostatic attraction, forming an adsorption film. Additionally, a tribochemical film containing FeOOH is formed, which is beneficial to friction reduction. Both the adsorption film and tribochemical films act as protective layers for the tribo-pair during the friction process, thereby reducing friction (Figure 8a). However, when the voltage is increased to -0.8 V, an increase in the variety of tribochemical reaction products leads to the formation of a more complex tribochemical film on the ball, including Fe_xO_y and P-O compounds (Figure 8b). Previous studies [47] have indicated that an increased content of Fe_xO_y in the tribochemical film is detrimental to friction reduction. Upon reversing the voltage direction to $+0.1$ V, the steel ball becomes the positive terminal. Owing to electrostatic repulsion, Li(PEG)^+ ions exhibit limited adsorption on the steel ball surface, leaving it unprotected and resulting in an elevated COF. Meanwhile, the tribochemical film contains Fe_xO_y , further contributing to the increased COF (Figure 8c).

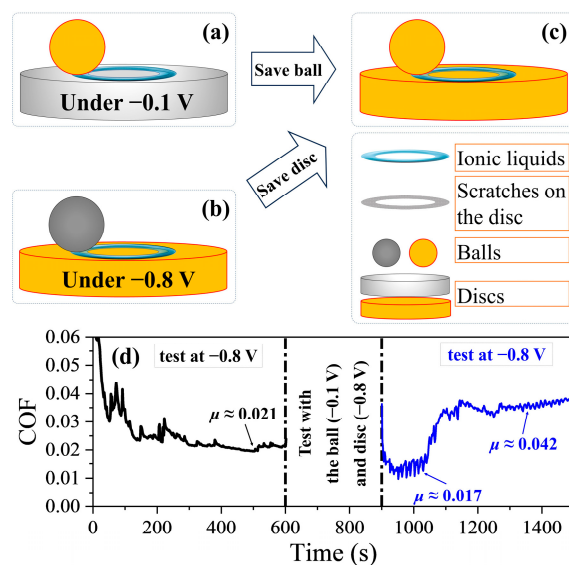


Figure 7. Procedures and results of the supplementary test, (a) friction test under -0.1 V and retaining the worn ball when stable lubrication was achieved, (b) friction test under -0.8 V and retaining the worn disc and the residual lubricant when stable lubrication was achieved, (c) friction test under -0.8 V with the worn ball (from -0.1 V test) and the worn disc (from -0.8 V test) on the same worn track, (d) friction test results before and after switching the tribo-pair.

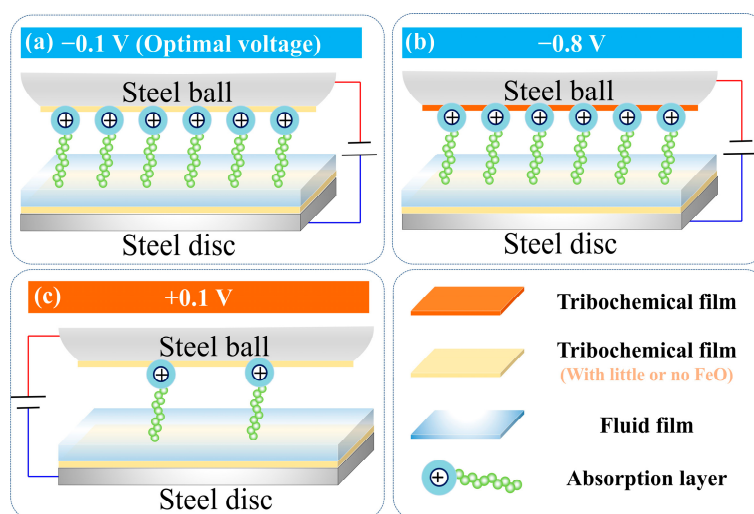


Figure 8. Schematic diagram of IL friction mechanism under (a) -0.1 V, (b) -0.8 V, and (c) $+0.1$ V.

In this study, we demonstrate that electrical stimulations can effectively regulate the friction performance of ions, offering significant advantages for at least two practical applications. The first application pertains to specific electrical environments. Under these conditions, appropriate lubricating materials can be chosen to achieve an optimal COF while ensuring friction stability based on their electrical regulation characteristics. The second application addresses varying working conditions, where suitable electrical stimulation signals can be used to regulate the friction performance of lubricants, allowing them to adapt to changing operational conditions.

5. Conclusions

The friction performance of $[\text{Li}(\text{PEG})]\text{PF}_6$ IL is significantly affected by the direction and magnitude of voltage stimulation in a ball-on-disc contact mode. A stimulation of -0.1 V leads to a significant reduction in friction to the superlubricity level. In contrast, stimulations of -0.8 V and $+0.1$ V show no detectable difference in COF compared to 0 V.

The underlying mechanism is concluded as follows: the voltage magnitude influences the COF by determining the types of substances in the tribochemical film formed on the ball, while the voltage direction influences the COF by affecting the adsorption behavior of Li(PEG)⁺ ions on the ball. At -0.1 V (the optimal voltage), Li(PEG)⁺ ions adsorb onto the ball via electrostatic attraction, forming an adsorption film of Li(PEG)⁺. Additionally, a tribochemical film containing FeOOH is formed. Both the adsorption film and tribochemical films act as protective layers for the tribo-pair, thereby reducing friction. At -0.8 V, the formation of Fe_xO_y within the tribochemical film results in an increase in friction compared to -0.1 V. At $+0.1$ V, the limited adsorption of Li(PEG)⁺ and the formation of Fe_xO_y on the ball surface contribute to the elevated COF compared to -0.1 V.

Author Contributions: Conceptualization: X.G., Q.S. and Y.L.; data curation, X.W.; funding acquisition, X.G.; investigation, Q.S. and H.L.; supervision, X.G., Q.S. and Y.L.; writing—original draft, X.W.; writing—review and editing, X.G., Q.S. and H.L. All authors have read and agreed to the published version of the manuscript.

Funding: This research was funded by the National Key R&D Program of China (2023YFB3405700) and the National Natural Science Foundation of China (52205180).

Data Availability Statement: The original contributions presented in the study are included in the article, further inquiries can be directed to the corresponding authors.

Conflicts of Interest: Author Qiuyu Shi was employed by the company State Grid Smart Grid Research Institute Co., Ltd. The remaining authors declare that the research was conducted in the absence of any commercial or financial relationships that could be construed as a potential conflict of interest.

Abbreviations

ILs	Ionic Liquids
COF	Coefficient of Friction
AFM	Atomic Force Microscope
PILs	Polymeric Ionic Liquids
ECR	Electrical Contact Resistance
WSD	Wear Scar Diameter
SEM	Scanning Electron Microscope
XPS	X-ray Photoelectron Spectroscopy
ML	Mixed Lubrication

References

1. Holmberg, K.; Andersson, P.; Erdemir, A. Global energy consumption due to friction in passenger cars. *Tribol. Int.* **2012**, *47*, 221–234. [[CrossRef](#)]
2. Whittle, M.; Trevelyan, J.; Tavner, P.J. Bearing currents in wind turbine generators. *J. Renew. Sustain. Energy* **2013**, *5*, 053128. [[CrossRef](#)]
3. He, F.; Xie, G.; Luo, J. Electrical bearing failures in electric vehicles. *Friction* **2020**, *8*, 4–28. [[CrossRef](#)]
4. Xie, G.; Guo, D.; Luo, J. Lubrication under charged conditions. *Tribol. Int.* **2015**, *84*, 22–35. [[CrossRef](#)]
5. Ge, X.; Chai, Z.; Shi, Q.; Liu, Y.; Wang, W. Graphene superlubricity: A review. *Friction* **2023**, *11*, 1953–1973. [[CrossRef](#)]
6. Matta, C.; Joly-Pottuz, L.; Bouchet, M.I.D.B.; Martin, J.M.; Kano, M.; Zhang, Q.; Goddard, W.A. Superlubricity and tribochemistry of polyhydric alcohols. *Phys. Rev. B* **2008**, *78*, 085436. [[CrossRef](#)]
7. Ge, X.; Li, J.; Luo, R.; Zhang, C.; Luo, J. Macroscale superlubricity enabled by the synergy effect of graphene-oxide nanoflakes and ethanediol. *ACS Appl. Mater. Interfaces* **2018**, *10*, 40863–40870. [[CrossRef](#)] [[PubMed](#)]
8. Ge, X.; Li, J.; Wang, H.; Zhang, C.; Liu, Y.; Luo, J. Macroscale superlubricity under extreme pressure enabled by the combination of graphene-oxide nanosheets with ionic liquid. *Carbon* **2019**, *151*, 76–83. [[CrossRef](#)]
9. Zhao, F.; Zhang, L.; Li, G.; Guo, Y.; Qi, H.; Zhang, G. Significantly enhancing tribological performance of epoxy by filling with ionic liquid functionalized graphene oxide. *Carbon* **2018**, *136*, 309–319. [[CrossRef](#)]
10. Li, H.; Wang, J.; Gao, S.; Chen, Q.; Peng, L.; Liu, K.; Wei, X. Superlubricity between MoS₂ monolayers. *Adv. Mater.* **2017**, *29*, 1701474. [[CrossRef](#)]
11. Gao, K.; Jiao, J.; Wang, Z.; Xie, G.; Luo, J. Superlubricity induced by partially oxidized black phosphorus on engineering steel. *Friction* **2023**, *11*, 1592–1605. [[CrossRef](#)]

12. Gao, K.; Lai, Z.; Jia, Q.; Zhang, B.; Wei, X.; Zhang, J. Bilayer a-C:H/MoS₂ film to realize superlubricity in open atmosphere. *Diam. Relat. Mater.* **2020**, *108*, 107973. [[CrossRef](#)]
13. Yu, G.; Gong, Z.; Jiang, B.; Wang, D.; Bai, C.; Zhang, J. Superlubricity for hydrogenated diamond like carbon induced by thin MoS₂ and DLC layer in moist air. *Diam. Relat. Mater.* **2020**, *102*, 107668. [[CrossRef](#)]
14. Zheng, Z.; Liu, X.; Yu, H.; Chen, H.; Feng, D.; Qiao, D. Insight into macroscale superlubricity of polyol aqueous solution induced by protic ionic liquid. *Friction* **2022**, *10*, 2000–2017. [[CrossRef](#)]
15. Han, T.; Zhang, C.; Chen, X.; Li, J.; Wang, W.; Luo, J. Contribution of a tribo-induced silica layer to macroscale superlubricity of hydrated ions. *J. Phys. Chem. C* **2019**, *123*, 20270–20277. [[CrossRef](#)]
16. Han, T.; Yi, S.; Zhang, C.; Li, J.; Chen, X.; Luo, J.; Banquy, X. Superlubrication obtained with mixtures of hydrated ions and polyethylene glycol solutions in the mixed and hydrodynamic lubrication regimes. *J. Colloid Interface Sci.* **2020**, *579*, 479–488. [[CrossRef](#)] [[PubMed](#)]
17. Liu, W.; Wang, H.; Liu, Y.; Zhang, C.; Luo, J. Controllable superlubricity system of polyalkylene glycol aqueous solutions under various applied conditions. *Macromol. Mater. Eng.* **2020**, *305*, 2000141. [[CrossRef](#)]
18. Zeng, Q.; Dong, G.; Martin, J.M. Green superlubricity of Nitinol 60 alloy against steel in presence of castor oil. *Sci. Rep.* **2016**, *6*, 29992. [[CrossRef](#)]
19. Jiang, Y.; Chen, L.; Xiao, C.; Zhang, S.; Zhang, C.; Zhou, N.; Qin, T.; Qian, L.; Zhang, J. How to improve superlubricity performance of diketone at steel interface: Effects of oxygen gas. *Friction* **2023**, *11*, 927–937. [[CrossRef](#)]
20. Reddyhoff, T.; Ewen, J.P.; Deshpande, P.; Frogley, M.D.; Welch, M.D.; Montgomery, W. Macroscale superlubricity and polymorphism of long-chain *n*-alcohols. *ACS Appl. Mater. Interfaces* **2021**, *13*, 9239–9251. [[CrossRef](#)]
21. Du, C.; Yu, T.; Wu, Z.; Zhang, L.; Shen, R.; Li, X.; Feng, M.; Feng, Y.; Wang, D. Achieving macroscale superlubricity with ultra-short running-in period by using polyethylene glycol-tannic acid complex green lubricant. *Friction* **2023**, *11*, 748–762. [[CrossRef](#)]
22. Arad, S.; Rapoport, L.; Moshkovich, A.; van Moppes, D.; Karpasas, M.; Golan, R.; Golan, Y. Superior biolubricant from a species of red microalga. *Langmuir* **2006**, *22*, 7313–7317. [[CrossRef](#)]
23. Tan, S.; Shi, H.; Du, X.; Wang, K.; Xu, H.; Wan, J.; Deng, K.; Zeng, Q.; Liu, Y. Electric field controlled superlubricity of fullerene-based host—Guest assembly. *Nano Res.* **2023**, *16*, 583–588. [[CrossRef](#)]
24. Li, H.; Wood, R.J.; Rutland, M.W.; Atkin, R. An ionic liquid lubricant enables superlubricity to be “switched on” in situ using an electrical potential. *Chem. Commun.* **2014**, *50*, 4368–4370. [[CrossRef](#)]
25. Zhang, Y.; Rutland, M.W.; Luo, J.; Atkin, R.; Li, H. Potential-dependent superlubricity of ionic liquids on a graphite surface. *J. Phys. Chem. C* **2021**, *125*, 3940–3947. [[CrossRef](#)]
26. Cai, H.; Zhang, C.; Li, F.; Liu, M.; Zhang, T.; Chu, H.; Liu, Z. Study on the microcosmic superlubricity mechanism of PVPA affected by metal cations. *Friction* **2023**, *11*, 1150–1164. [[CrossRef](#)]
27. Ye, C.F.; Liu, W.M.; Chen, Y.X.; Yu, L.G. Room-temperature ionic liquids: A novel versatile lubricant. *Chem. Commun.* **2001**, *21*, 2244–2245. [[CrossRef](#)] [[PubMed](#)]
28. Zhou, Y.; Qu, J. Ionic liquids as lubricant additives: A review. *ACS Appl. Mater. Interfaces* **2017**, *9*, 3209–3222. [[CrossRef](#)] [[PubMed](#)]
29. Ramezani, M.; Ripin, Z.M.; Jiang, C.-P.; Pasang, T. Superlubricity of materials: Progress, potential, and challenges. *Materials* **2023**, *16*, 5145. [[CrossRef](#)]
30. Lebedeva, O.; Kultin, D.; Kustov, L. Polymeric ionic liquids: Here, there and everywhere. *Eur. Polym. J.* **2023**, *203*, 112657. [[CrossRef](#)]
31. Cao, Z.; Xia, Y.; Liu, L.; Feng, X. Study on the conductive and tribological properties of copper sliding electrical contacts lubricated by ionic liquids. *Tribol. Int.* **2019**, *130*, 27–35. [[CrossRef](#)]
32. Gatti, F.; Amann, T.; Kailer, A.; Baltés, N.; Rühle, J.; Gumbsch, P. Towards programmable friction: Control of lubrication with ionic liquid mixtures by automated electrical regulation. *Sci. Rep.* **2020**, *10*, 17634. [[CrossRef](#)] [[PubMed](#)]
33. Yang, X.; Meng, Y.; Tian, Y. Effect of imidazolium ionic liquid additives on lubrication performance of propylene carbonate under different electrical potentials. *Tribol. Lett.* **2014**, *56*, 161–169. [[CrossRef](#)]
34. Ge, X.; Wu, X.; Shi, Q.; Song, S.; Liu, Y.; Wang, W. Study on the superlubricity behavior of ions under external electric fields at steel interfaces. *Langmuir* **2023**, *39*, 18757–18767. [[CrossRef](#)]
35. Song, Z.; Fan, M.; Liang, Y.; Zhou, F.; Liu, W. Lithium-based ionic liquids: In situ-formed lubricant additive only by blending. *Tribol. Lett.* **2013**, *49*, 127–133. [[CrossRef](#)]
36. Fan, M.; Liang, Y.; Zhou, F.; Liu, W. Dramatically improved friction reduction and wear resistance by in situ formed ionic liquids. *RSC Adv.* **2012**, *2*, 6824–6830. [[CrossRef](#)]
37. Lv, F.; Wang, W.; Zhang, B.; Jia, Q.; Gao, Y.; Wang, K. Black phosphorus quantum dots in aqueous environments as lubricants. *ACS Appl. Nano Mater.* **2023**, *6*, 13637–13645. [[CrossRef](#)]
38. Zeng, D.W.; Yung, K.C.; Xie, C.S. XPS investigation of the chemical characteristics of Kapton films ablated by a pulsed TEA CO₂ laser. *Surf. Coat. Technol.* **2002**, *153*, 210–216. [[CrossRef](#)]
39. Tan, H.; Zhai, D.; Kang, F.; Zhang, B. Synergistic PF₆[−] and FSI[−] intercalation enables stable graphite cathode for potassium-based dual ion battery. *Carbon* **2021**, *178*, 363–370. [[CrossRef](#)]
40. Strohmeier, B.R. Evaluation of polymeric standard reference materials for monitoring the performance of X-ray photoelectron spectrometers. *Appl. Surf. Sci.* **1991**, *47*, 225–234. [[CrossRef](#)]

41. Sleigh, C.; Pijpers, A.; Jaspers, A.; Coussens, B.; Meier, R.J. On the determination of atomic charge via ESCA including application to organometallics. *J. Electron Spectrosc. Relat. Phenom.* **1996**, *77*, 41–57. [[CrossRef](#)]
42. Beamson, G.; Briggs, D. High resolution monochromated X-ray photoelectron spectroscopy of organic polymers: A comparison between solid state data for organic polymers and gas phase data for small molecules. *Mol. Phys.* **1992**, *76*, 919–936. [[CrossRef](#)]
43. Glaser, T.; Meinecke, J.; Länger, C.; Luy, J.; Tonner, R.; Koert, U.; Dürr, M. Combined XPS and DFT investigation of the adsorption modes of methyl enol ether functionalized cyclooctyne on Si(001). *Chemphyschem* **2021**, *22*, 404–409. [[CrossRef](#)] [[PubMed](#)]
44. Kundu, S.; Wang, Y.; Xia, W.; Muhler, M. Thermal stability and reducibility of oxygen-containing functional groups on multiwalled carbon nanotube surfaces: A quantitative high-resolution XPS and TPD/TPR study. *J. Phys. Chem. C* **2008**, *112*, 16869–16878. [[CrossRef](#)]
45. Zhao, G.; Wu, X.; Li, W.; Wang, X. Hydroquinone bis(diphenyl phosphate) as an antiwear/extreme pressure additive in polyalkylene glycol for steel/steel contacts at elevated temperature. *Ind. Eng. Chem. Res.* **2013**, *52*, 7419–7424. [[CrossRef](#)]
46. NIST X-ray Photoelectron Spectroscopy Database. Available online: <https://srdata.nist.gov/xps/> (accessed on 26 March 2024).
47. Ge, X.; Wu, X.; Shi, Q.; Wang, W. Lubrication performances of polyalkylene glycols at steel interface under external electric fields. *Nanomaterials* **2022**, *12*, 2067. [[CrossRef](#)]

Disclaimer/Publisher’s Note: The statements, opinions and data contained in all publications are solely those of the individual author(s) and contributor(s) and not of MDPI and/or the editor(s). MDPI and/or the editor(s) disclaim responsibility for any injury to people or property resulting from any ideas, methods, instructions or products referred to in the content.